Insight into Compressive Behaviour of Schwarz-P Lattices Fabricated by Material Extrusion

P. Jameekornkul*, J. Wang*, A. Panesar*

* Department of Aeronautics, Imperial College London, SW7 2AZ, United Kingdom

Abstract

Lattice structures are increasingly being chosen for lightweight applications due to their high strength-to-weight ratio and energy absorption capability. This work investigates the mechanical performance of the Schwarz-Primitive (SP) lattices with a range of unit-cell sizes and relative densities. The SP lattices were fabricated using material extrusion with ASA (industrial grade) and ABS material, then tested along different orientations to build direction. Digital Image Correlation (DIC) was utilised to measure the local strain and deformation mechanism. The preliminary results indicate that stiffness and strength were related to densities abiding the Ashby-Gibson model in well-controlled tight bands, which will help inform design decisions for future adoption. Further experiments will be conducted to extend the finding of this study, gain a better understanding of graded lattices and provide insights on the potential use of fibre reinforcement in lattices.

Introduction

Cellular materials have been utilised for centuries in a wide variety of applications and are common in natural materials such as wood, bone, sponge, and coral. These can be regarded as a type of structure that consists of a network of solid struts or plates which form the edges and faces of cells [1]. One typical class of cellular material is lattice. Triply Periodic Minimal Surfaces (TPMS), a subset of the lattice structure, are derived from mathematics equations and allow design parameters and performance control in different disciplines [2]. Thus, TPMS lattice structures have gained much attention in many applications. Al-Ketan et al. [3] found that the sheet-TPMS based cellular structure showed superior mechanical performance compared to other types of lattice structures.

The capability of Additive Manufacturing (AM) technology allows these complex cellular structures to be realised and featured in many applications. A variety of studies [4]–[8] have been conducted to investigate lattice parameters and performance. The Gibson-Ashby model [1] is the most widely accepted, which predicts the properties of cellular structure based on the relative density of the cellular structure. Equation (1) and (2) show Gibson-Ashby's formulae for young's modulus and yield strength.

$$\frac{E^*}{E_0} = C_1\left(\frac{\rho^*}{\rho_0}\right)^{n_1} \quad (1)$$

$$\frac{\sigma^*}{\sigma_0} = C_5\left(\frac{\rho^*}{\rho_0}\right)^{n_5} \quad (2)$$

where E^*/E_0 and σ^*/σ_0 represent relative moduli and relative strength respectively. These mechanical properties are linked with the relative density using a power law, where the coefficient is C_i and exponent is n_i. Gibson, Ashby et al. provided the range of C_1 and C_5 for metal foams as [0.1-4.0] and [0.1-1.0] with $n_1 \sim 2$ and $n_5 \sim \frac{3}{2}$ (as plotted in Figure 1).

Obadimus and Kourousis [9] conducted a review of the compressive behaviour of AM lattice and showed that many studies focused on AM metallic lattice structure. However, as the polymer materials are gaining more attention for their cost and production time saving, some studies have been conducted on both the manufacturing process [10] and lattice design parameters [11][12]. Laban O. et al. [13] conducted a comparative experiment of

metal and polymer AM hexagonal cells. The general trends of compressive behaviour were similar. However, metal samples have a higher load-carrying magnitude due to higher yield strength in metal material. The polymer lattice produced by Fused Deposition Modelling (FDM) showed brittle fractures, while the metal samples showed excessive deformation with the ductile fractures. Despite defects and diffusion between building layers, FDM provides 80% time and 53% cost-efficient compared to direct metal laser sintering (DMLS).

Figure 1 summarises the experimental results of metallic SLM lattice structures [14] and shows that most of the experiments conducted were within the range for bending-dominated cellular structures provided by Gibson and Ashby. In addition, topologies seem to congregate within certain regions of the model. While the provided range is able to give an overall trend of cellular structure, the coefficient and exponent should be derived for specific lattice topology, materials and manufacturing process.

Table 1 summarises the C_i and n_i from experiments [7], [8], [15] conducted to investigate the TPMS lattice which were lying within a similar range. Unit cell types, materials properties, AM techniques and other experimental factors potentially cause the coefficient and exponent number to be different. This study will examine the Schwarz-P lattice properties and power-law parameters with based polymeric material fabricated by the material extrusion process. The polymeric material (ABS and ASA) and AM process were chosen for this study for their availability for general purposes.

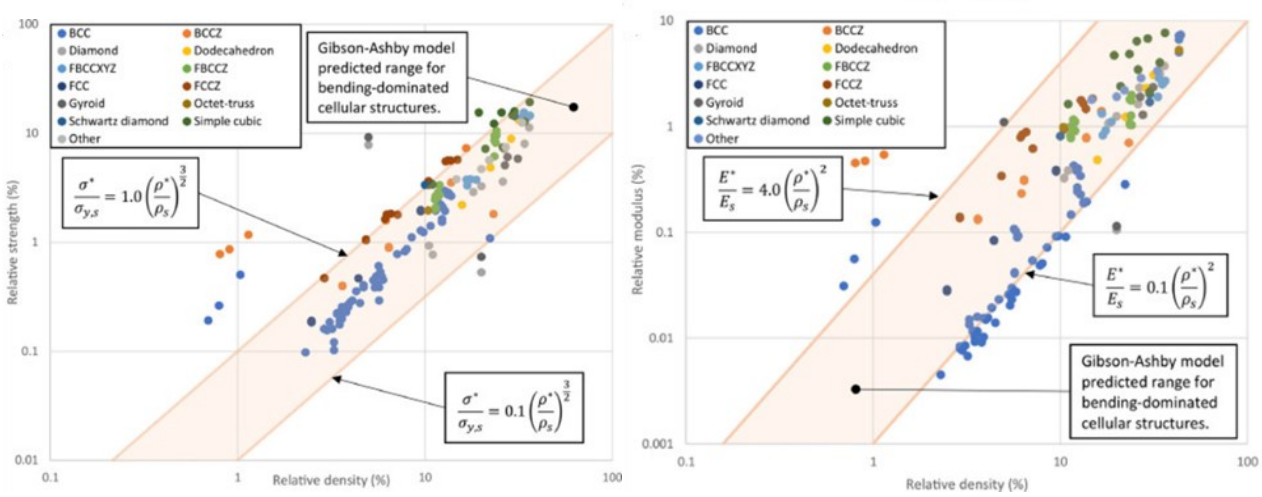

Figure 1: Summary of comparison between experimental data and the Gibson-Ashby model for (a) compressive strength and (b) Young's modulus [3]

Cell type	Material	Young's modulus		Yield strength	
		C	n	C	n
Primitive	316L stainless steel	0.228-0.253	1.416-1.472	0.818-0.843	1.443-1.557
Gyroid	Al–Si10–Mg	0.104-0.108	1.41-1.44	1.182-1.193	1.80-1.81
Gyroid	Ti–6Al–4V	0.19	1.71	1.31	1.83
Diamond		0.17	1.84	1.39	1.95

Table 1: Regression analysis of TPMS experimental data

Under uniaxial compression, the typical stress-strain response of a surface-based lattice is shown in Figure 2, described by Gibson and Ashby, including yield stress and elastic modulus. The response behaviour during plastic deformation is expected to differ for bending- and stretching-dominated structures (see more details on [1]). A few studies have been conducted to further the understanding of the AM lattice compression behaviour,

Rifaie A. et al. [16] investigated BCC polymer lattice structure, and Maskery I. et al. [11] investigated the double gyroid made of Al-Si10-Mg. Both studies are in good agreement with Figure 2, which supports the statement from [13] that base-material metal and polymer have similar compressive behaviour. A study of polymer AM TPMS lattices was conducted and suggested stretching-dominated deformation for SP structure, unlike gyroid and diamond, which portrayed bending dominated [17].

Further analysis reveals different failure modes observed throughout the studies: [16] investigated bending and buckling of different sub-types of BCC lattices, and [11] showed a few successive collapses, crack propagation parallel to the applied load in the larger cell sizes and diagonal shear in the smallest cell sizes of double gyroid (Figure 3). However, the number of studies on failure modes influenced by lattice topologies and design parameters is still limited. Thus, this study performed a preliminary observation on the failure modes of SP lattice structure fabricated by the material extrusion technique.

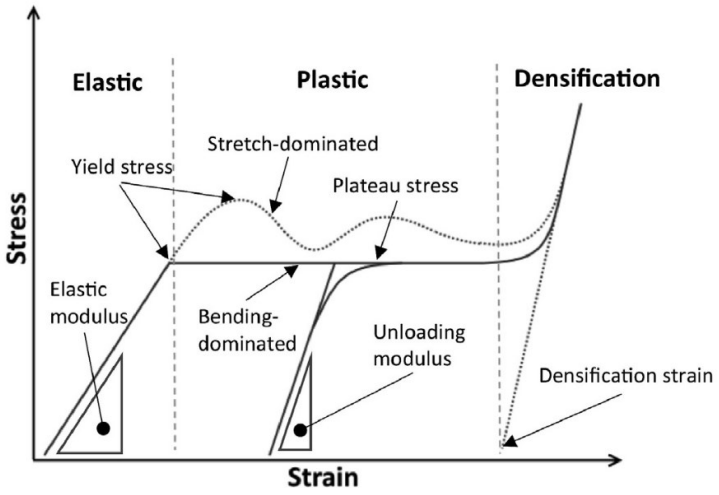

Figure 2: General compressive behaviour of stretch and bending-dominated lattice structures (reprinted from [14])

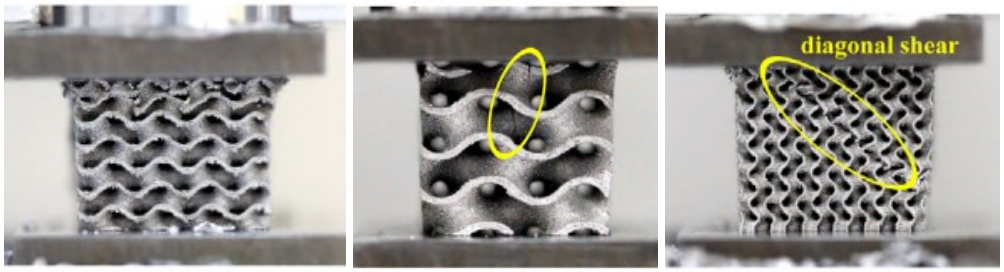

Figure 3: Compressive failure modes of double gyroids lattice structure (reprint from [11])

Apart from the failure modes which potentially affected by cell sizes [11], the cell sizes could be a factor to consider for improving the surface roughness and print quality. The staircase effect is caused by the layer-by-layer printing technique and leads to high surface roughness, especially on curved surfaces [18]. Pérez et al. [19] stated that the wall thickness and layer height worsen the surface roughness if either or both values are increased. Therefore, considering the fixed wall thickness and layer height, the samples with larger cell size has a tendency to have a better surface finish compared to smaller cell size at the same volume fraction and bounding box size. This study will be conducted at various cell sizes to understand the surface roughness results.

Methodology

The material extrusion technique is chosen to fabricate the parts. The Fortus 450mc – an industry grade printer - is selected due to its capability to deliver accurate and reliable performance. For further understanding of the effects of manufacturing, Ultimaker 3 Extended is chosen for its accessibility to most general users. The lattice structures are designed by in-house software developed by Janos P. [6] according to the test matrix shown in Table 2 and then fabricated by the material extrusion process. The volume fraction (vf) is chosen between 0.2-0.5 as beyond the volume fraction of 0.5, and the lattice would transition from open to closed cell, which is beyond the consideration of this study. In addition, [3] noted that the effect of cell topologies is more evident at smaller relative density.

It should be noted that the parts fabricated by AM, specifically the material extrusion process, have shown anisotropy properties [20], [21]. Zaldivar R. et al. proposed that the build orientations affect the ULTEM 9085 microstructure, mechanical, and thermal properties [5]. Thus, to preliminarily observe the effect of build orientation, the compression tests will be conducted in two directions: X direction - performed in the direction perpendicular to the print direction and Z direction – parallel to the print direction. For each type of material, the test matrix (Table 2) will be tested in two different directions two times. The mechanical properties of commercial materials which were used in fabrication are provided in Table 3. The lattice structures with 5 mm cell size were fabricated for printability evaluation. The 5mm samples were not fully printed due to the small layer thickness required for the thin wall part. While the volume fraction is considered the most critical factor, cell size plays an essential role in the design and manufacturing limitations.

Materials	Stratasys ASA (Fortus 450mc)		
	Ultimaker ABS (Ultimaker 3 Extended)		
Unit cell size	7.5 mm	10 mm	15 mm
Tessellation	4x4x4	3x3x3	3x3x3
Relative density	0.25, 0.35, 0.5	0.2, 0.35, 0.5	0.2, 0.35, 0.5

Table 2: Test matrix

Materials	**Yield strength (MPa)**		**Modulus (GPa)**	
	Compression	Tensile	Compression	Tensile
Stratasys ASA	75.4	32.8	2.05	2.14
Ultimaker ABS	65	39	2.5	1.681

Table 3: Material properties[22],[23]

Compression tests will be performed to obtain the experimental moduli and strength of the lattice structures, which are adopted to represent the stiffness and strength values, respectively. The experiment will be performed using the 50kN Instron 5969 machine according to the ASTM D695-15 [24] at the constant rate of 1mm/min. The time, force, displacement, and video of the experiments will be recorded for further analysis. The Digital Image Correlation (DIC) technique is used to measure the mechanical properties during the deformation. From the stress-strain curve obtained, the first peak of stress value is regarded as yield strength, and the young's modulus will be computed between 0.05-0.2 strain. The regression analysis will be performed on the yield stress and young's modulus to observe the power-law relationship.

Since material extrusion is a thermal process, the porosity could introduce pores and voids, affecting mechanical properties [25]. Wang et al.'s study showed that the amount of porosity observed was different given the specimen printed by the same printing control due to random errors within process controls, e.g., material distribution within the filament. Therefore, despite the printing parameters being fixed, the property of the lattice structure may fluctuate. In order to reflect the lattice's mechanical property precisely, the reliable region will be identified using the band where the exponent n is fixed. At the same time, the coefficient ranges from lower C_l to upper boundary C_u. Figure 4 shows the derivation of the relative modulus band plotted on the log scale graph. The optimisation of parameter n is defined as

$$\min_{n \geq 0} \ln C_u - \ln C_l \tag{3}$$
$$s.t. \ln C_l + nx_i \leq y_i \leq \ln C_u + nx_i \, , i = 1,2,3 \ldots N$$

where i denotes the index of data and N is the total number of data. In order to ensure that at least 90% of data falls in the prediction band, the constraint was determined as the lower and upper bound of the 90% confidence interval of all data obtained.

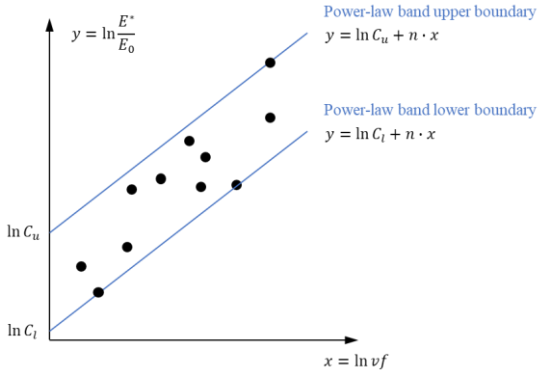

Figure 4: The power-law band on the log scale graph

Results and Discussions

The reliable bands are identified by the proposed post-processing method. Figure 5 shows the bands for SP lattice structure with ASA-based material and Figure 6 with the based material of ABS. As seen from both figures, the bands broadly captured the trend of the experimental results, which can be described by Ashby and Gibson's power law and parameters in Table 4.

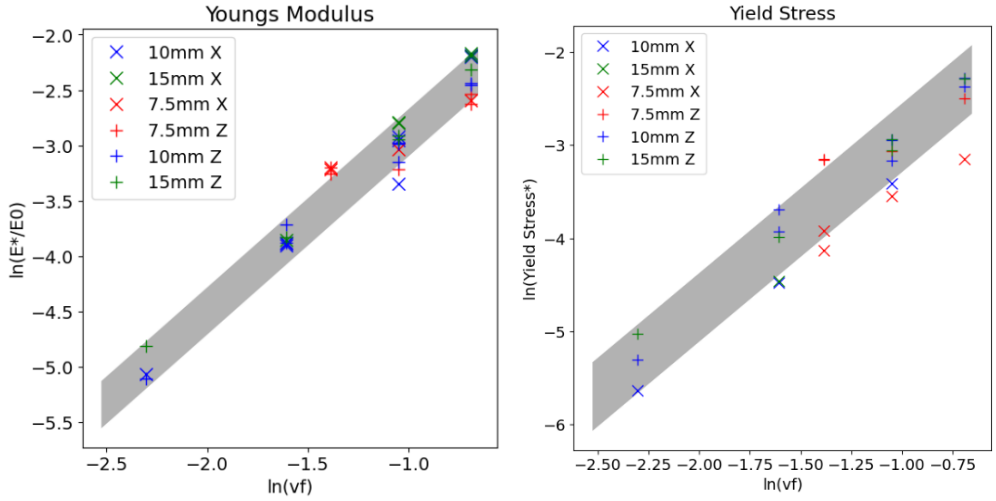

Figure 5: Reliable band of ASA-based material by Fortus450 on log-scaled graph
(a) Young Modulus (b) Yield Stress

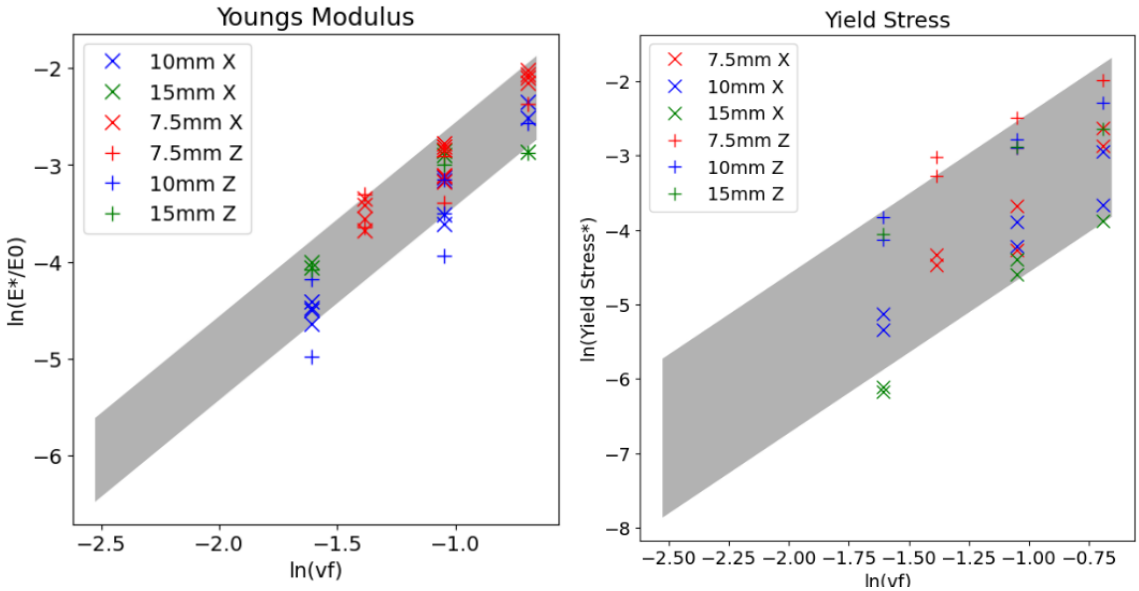

Figure 6: Reliable band of ABS-based material by Ultimaker on log-scaled graph (a) Young Modulus (E) (b) Yield Stress (σ)

Materials	Property	C_l	C_u	n
ASA	E	0.23	0.35	1.6
	σ	0.23	0.48	1.8
ABS	E	0.24	0.57	1.9
	σ	0.09	0.76	2.2

Table 4: Parameters of reliable bands

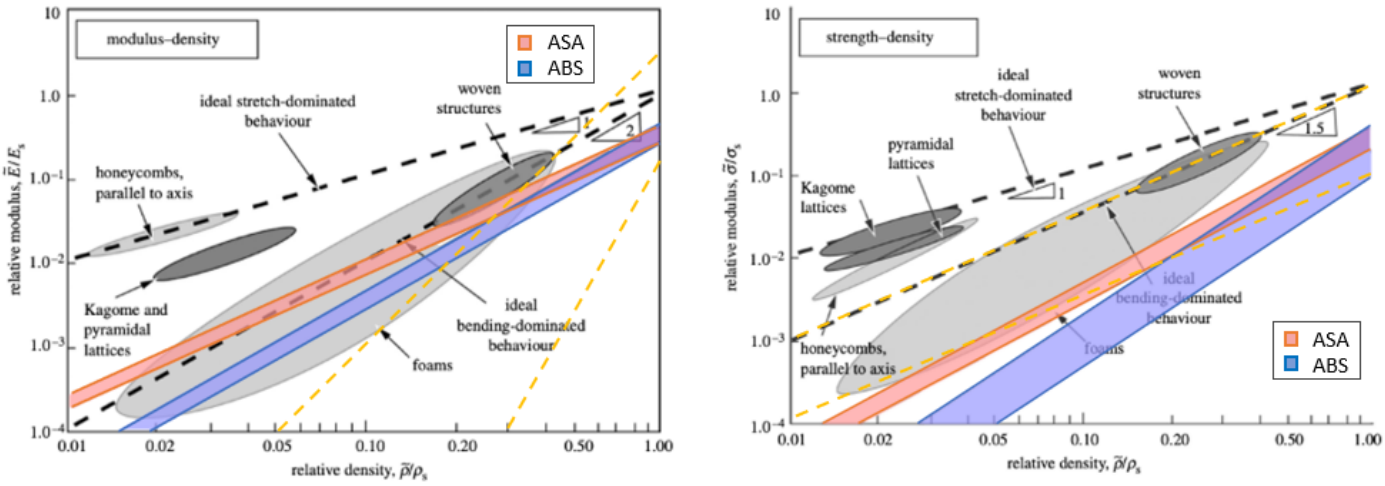

Figure 7: Prediction band in comparison to Gibson-Ashby prediction model (Redrawn and adapted from [26],[14]) (a) Young's modulus (b) Yield strength

Figure 7 shows a comparison between identified bands and literature. The yellow bands indicate the range for metallic open-cellular structure mentioned in [14]. The red band represents the prediction derived from ASA material, and the blue band represents the ABS material. For modulus, the slope of ABS is comparable to the ideal bending-dominated, while the slope of ASA is slightly less steep. While the slope of the same lattice topology is expected to be similar, this could be due to the geometry difference compared to the design and other imperfections. Therefore, further investigation should be conducted on another type of material under printing

process control. In addition, to confirm the effect of lattice topology, another type of lattice unit cell should be investigated and compared.

For strength, the ASA band have a similar gradient to the bending-dominated line, while the ABS band is slightly steeper. Therefore, the ideal stretch-dominated line cannot predict the SP lattice's properties obtained from these preliminary experiments. Similar to the modulus plot, further investigation is required to confirm the effect of cell topology and material properties. It can be established that the parts produced by the Ultimaker 3 extended printer contain more fluctuating mechanical properties than an industrial printer. While the relative young's moduli were lying closely, the yield strength band was more spread out, thus, a wider prediction band.

Apart from the printing process and material effect, the build direction is observed during the experiment. Figure 5 and Figure 6 show that there is a notable difference between X and Z directions in yield strength σ. To investigate the relationship between σ_z and σ_x, the linear regression is conducted and indicated that the ratio between σ_z and σ_x remains consistent as 2.26 (with $r^2 = 0.94$) for ASA material with Fortus450mc and 2.12 (with $r^2 = 0.96$) for ABS material produced by the Ultimaker 3 extended.

Figure 8 shows the example of compressive behaviour obtained from this study which complies with the general behaviour discussed in Figure 2. Noted that the stress is the load per unit area and strain is displacement per unit length, the load-displacement curve could reflect the stress-strain curve. However, samples tested transverse to the build direction show less yield strength value and oscillation between each layer since the samples tend to fail. Therefore, the build orientation significantly affects the compressive properties and the quality of printed parts.

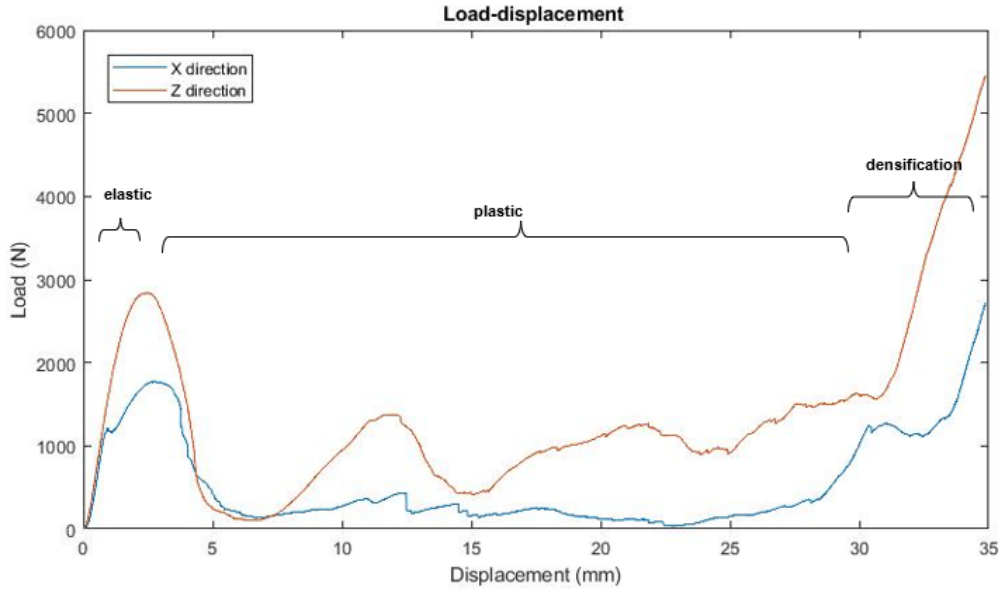

Figure 8: Load-displacement plot of UC=15mm and vf=0.2 tested in a different direction

At the early stage of the elastic region, both x and z direction testings' load-displacement linearly increase before reaching the yield stress and entering the plastic deformation. For samples tested in the z-direction, horizontal cracks originated at the thin part of the structure where the bonding between layers is weak. As the strain increases, two different failure modes were observed:

1. The successive layer-by-layer collapse was observed in the plastic region. For lattice with 3x3x3 tessellation, the middle layer started the bending deformation (Figure 9), while the two layers in the middle of the 4x4x4 lattice started deforming simultaneously. This failure mode occurred when the unit cell size was small, and the volume fraction was low.

2. For high volume fraction and larger unit cell size, diagonal shear deformation was observed at 45° of the compression axes (Figure 10(a)) or formed into X- or V-shaped direction (Figure 10(b)). This failure is more noticeable in the structure produced by the industrial printer, potentially due to a better interlaminar bond between layers.

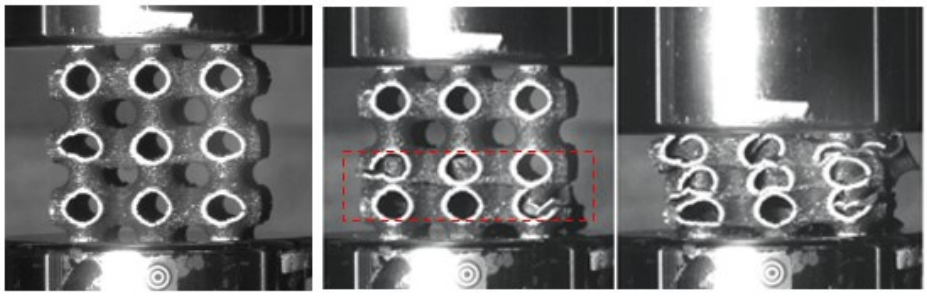

Figure 9: Layer-by-layer deformation

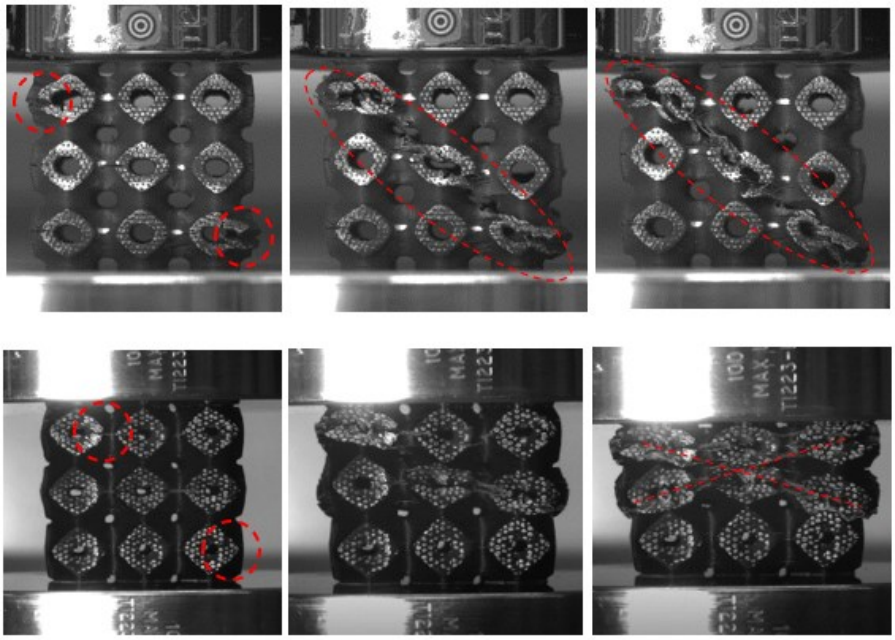

Figure 10: Compressive failure behaviour (a-c) Diagonal shear deformation in 45° direction (d-f) Diagonal shear deformation in x-shaped direction

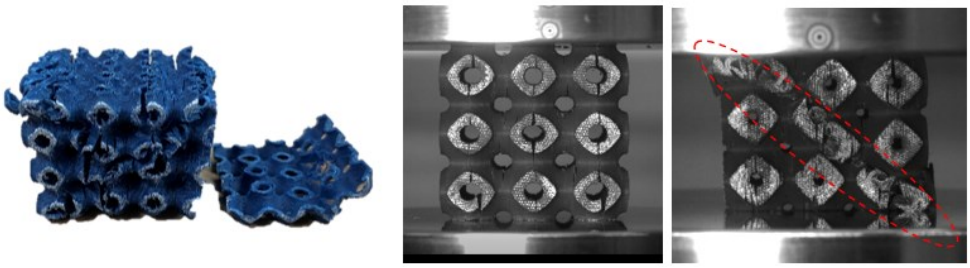

Figure 11: Example of compressive failures tested in the X-direction (a) Delamination (b) Vertical cracks (c) Diagonal shear

Similar to the z-direction, the x-direction tested samples show two failure modes: successive and shear failure. However, additional behaviour was spotted due to changing the test direction. The vertical cracks formed at the thinnest part of the experiments tested in the x-direction. As the strain increases, the delamination or in-

plane debonding was observed (Figure 11 (a)) due to the vertical crack propagation caused by inter-beads porosity. This separation occurred in most x-direction cases except in large cells with high relative density, which shows 45° diagonal shear failure (Figure 11(c)). While the testing in the X-direction clearly exhibited delamination failure, the z-direction test, which was performed perpendicular to the build direction, exhibited more than one failure mode depending on lattice design parameters (size and volume fraction).

Figure 12 summarises the failure modes observed considering the lattice design parameters (UC size and volume fraction). As mentioned previously, the shear deformation was observed in a higher volume fraction and a larger unit cell, while the layer-by-layer deformation occurred on the lower side. However, further microstructure analysis should be conducted to understand the compressive behaviour fully.

Figure 13 shows printed parts with the same volume fraction in comparison. The printed by the Fortus 450mc printer has a lower surface roughness compared to the ABS sample printed by the Ultimaker 3 extended. In comparison to the larger unit cell size, the part with 10 mm has a smoother surface compared to the smaller unit cell size due to the layer being allowed to continuously bonded in a larger cell size structure.

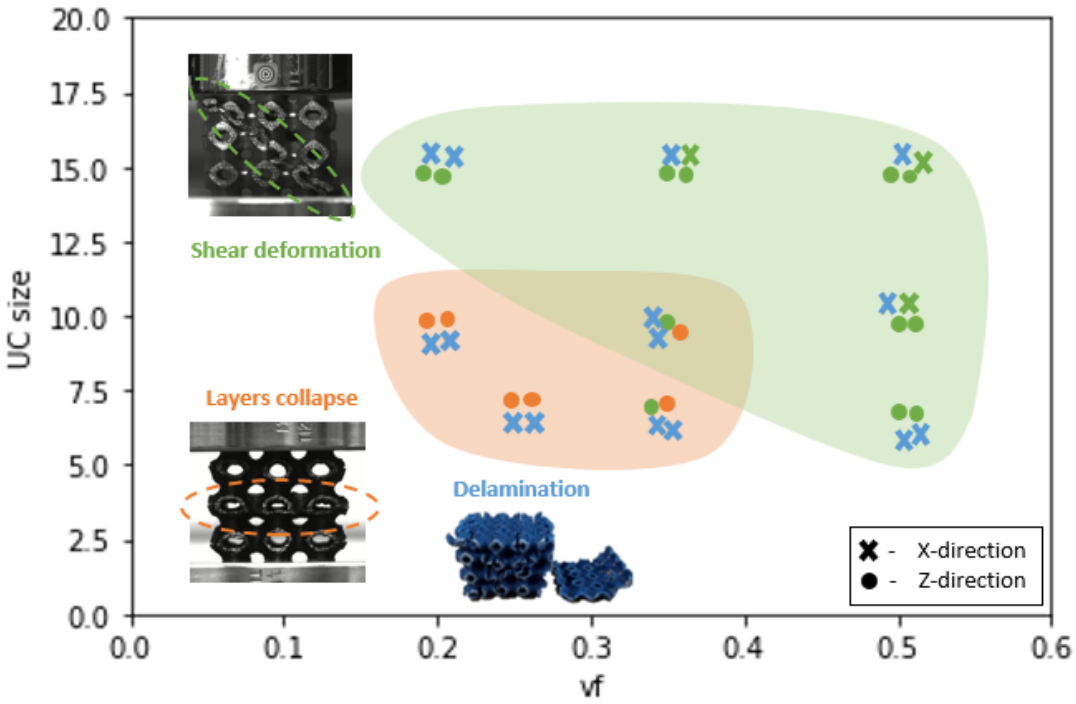

Figure 12: General failure mode observed in relationship with UC size and volume fraction

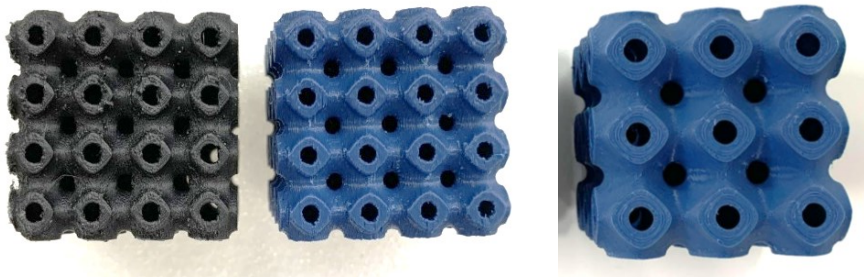

Figure 13: Examples printed parts (a) ABS vf=0.35 UC=7.5 mm (b) ASA vf=0.35 UC=7.5 mm (c) ASA vf=0.35 UC=10mm

Conclusion

An investigation of the compression behaviour of lattice structures produced by the material extrusion process was conducted. Various parameters were investigated, including the based materials type, the printing process, printability and quality of products, lattice design parameters, mechanical behaviour, and the failure mechanism under compressive load. The study shows that the volume fraction of lattice influences the mechanical properties the most, which could be explained by the power-law relationship and derived into the prediction band. The derived relationship could be used for many AM applications and design optimisation, for example, volume fraction control within the design to achieve the optimal mechanical properties. The current preliminary results suggested a slightly different slope for the same SP lattices potentially caused by imperfections in the printing process. Thus, further investigations will be conducted on different lattice topologies and materials.

The SP lattice structures were mainly deformed by diagonal shear at high volume fractions and larger sizes. On the other hand, successive collapse and crack propagation were observed on the lattice structure with low volume fraction and smaller size. For the structure tested in the Z-direction, vertical cracks were observed and then the structure was deformed by delamination in between printed layers. Further microstructural characterisation analysis is planned to detect and understand the failure behaviour on a micro-scale. In addition, the qualitative approach should be measured by optical profilometry to evaluate the surface quality in material extrusion.

The materials' properties, lattice parameters and printing process influence the mechanical properties; therefore, the prediction model is slightly different for each material, printer, lattice topology and design. Further investigation should be conducted on metallic and polymeric AM lattice comparison, an effect of path-planning which can potentially be extended to fibre reinforcement application.

Acknowledgements

Mark Forest and Peter Greaves from Off-shore Renewable Energy (ORE) Catapult, UK who provided input and guidance throughout the study.

Reference

[1] L. J. Gibson and M. F. Ashby, *Cellular Solids*. Cambridge University Press, 1997. doi: 10.1017/CBO9781139878326.

[2] A. Panesar, M. Abdi, D. Hickman, and I. Ashcroft, “Strategies for functionally graded lattice structures derived using topology optimisation for Additive Manufacturing,” *Addit Manuf*, vol. 19, pp. 81–94, Jan. 2018, doi: 10.1016/J.ADDMA.2017.11.008.

[3] O. Al-Ketan, R. Rowshan, and R. K. Abu Al-Rub, “Topology-mechanical property relationship of 3D printed strut, skeletal, and sheet based periodic metallic cellular materials,” *Addit Manuf*, vol. 19, pp. 167–183, Jan. 2018, doi: 10.1016/J.ADDMA.2017.12.006.

[4] M. Zhao, F. Liu, G. Fu, D. Z. Zhang, T. Zhang, and H. Zhou, “Improved Mechanical Properties and Energy Absorption of BCC Lattice Structures with Triply Periodic Minimal Surfaces Fabricated by SLM,” *Materials*, vol. 11, no. 12, 2018, doi: 10.3390/ma11122411.

[5] R. J. Zaldivar, D. B. Witkin, T. McLouth, D. N. Patel, K. Schmitt, and J. P. Nokes, “Influence of processing and orientation print effects on the mechanical and thermal behavior of 3D-Printed ULTEM® 9085 Material,” *Addit Manuf*, vol. 13, pp. 71–80, Jan. 2017, doi: 10.1016/J.ADDMA.2016.11.007.

[6] J. Plocher and A. Panesar, “Effect of density and unit cell size grading on the stiffness and energy absorption of short fibre-reinforced functionally graded lattice structures,” *Addit Manuf*, vol. 33, p. 101171, May 2020, doi: 10.1016/J.ADDMA.2020.101171.

[7] C. Yan, L. Hao, A. Hussein, and P. Young, “Ti–6Al–4V triply periodic minimal surface structures for bone implants fabricated via selective laser melting,” *J Mech Behav Biomed Mater*, vol. 51, pp. 61–73, Nov. 2015, doi: 10.1016/J.JMBBM.2015.06.024.

[8] C. Lu, C. Zhang, P. Wen, and F. Chen, “Mechanical behavior of Al–Si10–Mg gyroid surface with variable topological parameters fabricated via laser powder bed fusion,” *Journal of Materials Research and Technology*, vol. 15, pp. 5650–5661, Nov. 2021, doi: 10.1016/J.JMRT.2021.11.008.
[9] S. O. Obadimu and K. I. Kourousis, “Compressive Behaviour of Additively Manufactured Lattice Structures: A Review,” *Aerospace*, vol. 8, no. 8, 2021, doi: 10.3390/aerospace8080207.
[10] G. Dong, G. Wijaya, Y. Tang, and Y. F. Zhao, “Optimizing process parameters of fused deposition modeling by Taguchi method for the fabrication of lattice structures,” *Addit Manuf*, vol. 19, pp. 62–72, Jan. 2018, doi: 10.1016/J.ADDMA.2017.11.004.
[11] I. Maskery, N. T. Aboulkhair, A. O. Aremu, C. J. Tuck, and I. A. Ashcroft, “Compressive failure modes and energy absorption in additively manufactured double gyroid lattices,” *Addit Manuf*, vol. 16, pp. 24–29, Aug. 2017, doi: 10.1016/J.ADDMA.2017.04.003.
[12] G. K. Maharjan, S. Z. Khan, S. H. Riza, and S. H. Masood, “Compressive Behaviour of 3D Printed Polymeric Gyroid Cellular Lattice Structure,” *IOP Conf Ser Mater Sci Eng*, vol. 455, p. 12047, Dec. 2018, doi: 10.1088/1757-899x/455/1/012047.
[13] O. Laban, E. Mahdi, S. Samim, and J.-J. Cabibihan, “A Comparative Study between Polymer and Metal Additive Manufacturing Approaches in Investigating Stiffened Hexagonal Cells,” *Materials*, vol. 14, p. 883, Jun. 2021, doi: 10.3390/ma14040883.
[14] T. Maconachie *et al.*, “SLM lattice structures: Properties, performance, applications and challenges,” *Materials and Design*, vol. 183. 2019. doi: 10.1016/j.matdes.2019.108137.
[15] X. Guo *et al.*, “Enhancement in the mechanical behaviour of a Schwarz Primitive periodic minimal surface lattice structure design,” *Int J Mech Sci*, vol. 216, p. 106977, Feb. 2022, doi: 10.1016/J.IJMECSCI.2021.106977.
[16] M. al Rifaie, A. Mian, and R. Srinivasan, “Compression behavior of three-dimensional printed polymer lattice structures,” *Proceedings of the Institution of Mechanical Engineers, Part L: Journal of Materials: Design and Applications*, vol. 233, no. 8, pp. 1574–1584, 2019, doi: 10.1177/1464420718770475.
[17] I. Maskery *et al.*, “Insights into the mechanical properties of several triply periodic minimal surface lattice structures made by polymer additive manufacturing,” *Polymer (Guildf)*, vol. 152, pp. 62–71, Sep. 2018, doi: 10.1016/J.POLYMER.2017.11.049.
[18] M. Pérez, A. García-Collado, D. Carou, G. Medina-Sánchez, and R. Dorado-Vicente, “On surface quality of engineered parts manufactured by additive manufacturing and postfinishing by machining,” *Addit Manuf*, pp. 369–394, Jan. 2021, doi: 10.1016/B978-0-12-818411-0.00015-X.
[19] M. Pérez, G. Medina-Sánchez, A. García-Collado, M. Gupta, and D. Carou, “Materials Surface Quality Enhancement of Fused Deposition Modeling (FDM) Printed Samples Based on the Selection of Critical Printing Parameters,” 2018, doi: 10.3390/ma11081382.
[20] N. S. Hmeidat, R. C. Pack, S. J. Talley, R. B. Moore, and B. G. Compton, “Mechanical anisotropy in polymer composites produced by material extrusion additive manufacturing,” *Addit Manuf*, vol. 34, p. 101385, Aug. 2020, doi: 10.1016/J.ADDMA.2020.101385.
[21] M. Somireddy and A. Czekanski, “Anisotropic material behavior of 3D printed composite structures – Material extrusion additive manufacturing,” *Mater Des*, vol. 195, p. 108953, Oct. 2020, doi: 10.1016/J.MATDES.2020.108953.
[22] Stratasys, “ABS Black safety Datasheet,” Sep. 2021. Accessed: Jun. 23, 2022. [Online]. Available: https://support.stratasys.com/en/materials/fdm/asa
[23] Ultimaker, “Ultimaker ABS Technical data sheet,” Apr. 2022. Accessed: Jun. 23, 2022. [Online]. Available: https://support.ultimaker.com/hc/en-us/articles/360012759139-Ultimaker-ABS-TDS
[24] ASTM International, “Standard Test Method for Compressive Properties of Rigid Plastics 1”, doi: 10.1520/D0695-15.
[25] Wang, L. Zhao, Fuh, and Lee, “Effect of Porosity on Mechanical Properties of 3D Printed Polymers: Experiments and Micromechanical Modeling Based on X-Ray Computed Tomography Analysis,” *Polymers (Basel)*, vol. 11, p. 1154, Jun. 2019, doi: 10.3390/polym11071154.
[26] M. Ashby, “The Properties of Foams and Lattices,” *Philos Trans A Math Phys Eng Sci*, vol. 364, pp. 15–30, Jun. 2006, doi: 10.1098/rsta.2005.1678.